Room temperature tunneling magnetoresistance in magnetite based junctions: Influence of tunneling barrier

D. Reisinger,[1,*] P. Majewski,[1] M. Opel,[1] L. Alff,[1,†] and R. Gross[1]

[1] *Walther-Meißner-Institut, Bayerische Akademie der Wissenschaften, Walther-Meißner Str. 8, 85748 Garching, Germany*

(Dated: received March 24, 2004)

Magnetite (Fe_3O_4) based tunnel junctions with turret/mesa structure have been investigated for different barrier materials ($SrTiO_3$, $NdGaO_3$, MgO, SiO_2, and Al_2O_{3-x}). Junctions with a Ni counter electrode and an aluminium oxide barrier showed reproducibly a tunneling magnetoresistance (TMR) effect at room temperature of up to 5% with almost ideal switching behavior. This number only partially reflects the intrinsic high spin polarization of Fe_3O_4. It is considerably decreased due to an additional series resistance within the junction. Only SiO_2 and Al_2O_{3-x} barriers provide magnetically decoupled electrodes as necessary for sharp switching. The observed decrease of the TMR effect as a function of increasing temperature is due to a decrease in spin polarization and an increase in spin-scattering in the barrier. Among the oxide half-metals magnetite has the potential to enhance the performance of TMR based devices.

PACS numbers: 75.70.-i, 85.75.-d

INTRODUCTION

Magnetic random access memory (MRAM) devices based on magnetic tunnel junctions (MTJ) using ferromagnetic metals and alloys with limited spin polarization will be implemented in next generation computer memory. Beyond purely storage usage, MTJs can at the same time be used as programmable logic elements [1]. While the device preparation techniques using simple metals and alloys are at least in principle well known, from the point of view of magnetic properties half metallic materials certainly are superior to classical ferromagnetic metals. Magnetite (Fe_3O_4) is an interesting candidate, because it has been predicted to be a half-metal even at room temperature due to its high ordering temperature of 860 K [2, 3]. Indeed, spin-resolved photoelectron spectroscopy on magnetite thin films has recently revealed a spin polarisation near the Fermi edge of up to 80% at room temperature [4]. In contrast, in MTJs only very small TMR effects have been observed [5, 6, 7, 8] with a maximum effect of 14% [9]. Therefore, it is important to understand the behavior of magnetite at the electrode/barrier interfaces, the influence of the tunneling barrier itself, and the magnetic coupling through thin barriers.

In this paper we report measurements of MTJs based on epitaxial magnetite thin films on MgO(001) single crystal substrates. As tunnel barrier the five materials MgO, $SrTiO_3$, $NdGaO_3$, SiO_2, and Al_2O_{3-x} have been investigated. As counter-electrode Ni was used with about 33% spin polarisation as known from tunneling measurements [10]. The whole thin film structure was grown by pulsed laser deposition (PLD) and electron beam evaporation in an ultra high vacuum system. The tunnel junctions with areas ranging from $10 \times 10\,\mu m^2$ to $20 \times 40\,\mu m^2$ were fabricated by optical lithography and ion beam etching. The magnetic properties, in particular the coupling of the electrodes through the barrier, have been studied by SQUID magnetometry. The magnetotransport behavior of these MTJs was measured as a function of temperature and applied magnetic field.

EXPERIMENTAL TECHNIQUES

The thin films were fabricated in an ultra high vacuum (UHV) laser ablation system with in-situ electron beam evaporation. The magnetite thin films were grown epitaxially on MgO single crystal substrates, mostly with an underlying epitaxial TiN buffer layer. Details about the whole process including in-situ reflection high energy electron diffraction (RHEED) and laser substrate heating are described in [11, 12, 13]. To enhance the surface quality a telescope optics for the laser beam has been developed, so that for each material the optimal energy density in combination with an optimal focus could be easily achieved. This was especially important for getting smooth surfaces without droplets which may lead to short circuits through the tunnel barrier. The surface quality was probed in-situ with an Omicron atomic force microscope, the crystal properties and film thickness with a Bruker/AXS high resolution X-ray-diffractometer, and the magnetic properties with a Quantum Design superconducting quantum interference device (SQUID) magnetometer. The magneto-transport measurements were performed in an Oxford cryostat system with variable temperature insert and a 10 Tesla superconducting magnet. The magnetite thin films achieved nearly the same properties as single crystal bulk material with respect to magnetization on the Verwey-transition behavior [14]. Such high-quality thin films seem to be one of the key prerequisites in order to obtain TMR devices with desired performance.

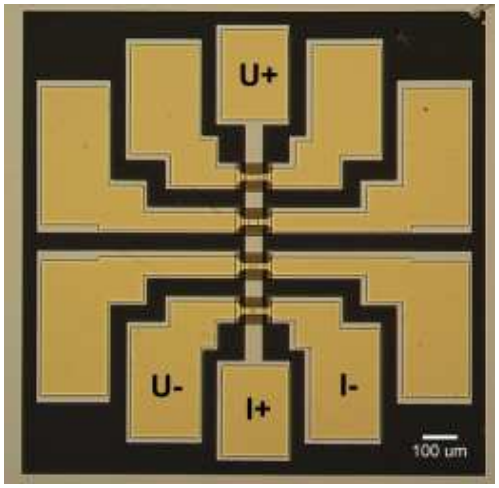

(a)

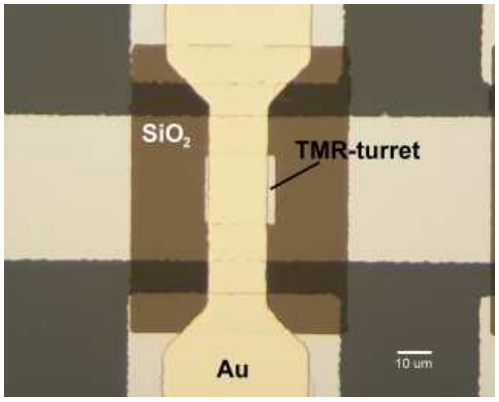

(b)

Figure 1: Optical microscope images of a completed TMR-bridge (a) with four TMR-contacts (called turrets), and a zoom-view (rotated by 90°) of a single turret with a size of $20 \times 20\,\mu\mathrm{m}^2$ (b).

On top of the 40 to 50 nm thin magnetite films, 2 to 7 nm thin layers serving as tunnel barriers are deposited. Five different materials were used: MgO, $SrTiO_3$ and $NdGaO_3$ have been fabricated by PLD from stoichiometric targets, SiO_2 and Al layers were deposited by electron beam evaporation in UHV. During PLD growth the Ar-atmosphere was 10^{-3} mbar, and the substrate temperature was 330°C. The only material growing epitaxially on Fe_3O_4 is MgO as confirmed by the corresponding RHEED pattern. Epitaxial growth of MgO is also achieved at room temperature for a pure oxygen atmosphere (10^{-3} mbar). The SiO_2 and Al layers were deposited without breaking the UHV after the magnetite deposition. Both materials are grown at room temperature. Afterwards the Al was oxidized in pure oxygen to form the insulating Al_2O_{3-x}. $SrTiO_3$, $NdGaO_3$, SiO_2, and Al_2O_{3-x} all form amorphous layers on magnetite due to the large crystal lattice mismatch. In a further step, a 40 nm Ni layer was deposited in situ as second magnetic electrode by electron beam evaporation in UHV at room temperature.

Starting from these multilayers, tunnel junctions have been fabricated using optical lithography and ion beam etching. The complex production process consists of roughly 35 critical steps. After careful optimization a yield of more than 50% of reproducible TMR-contacts was achieved corresponding to a yield of 98% for each step. This high reproducibility is an important prerequisite for a reliable analysis of the TMR-effect. As show in Fig. 1(a) one measurement bridge contains four tunnel junction in form of small ‚turrets' with areas ranging from $10 \times 10\,\mu\mathrm{m}^2$ to $20 \times 40\,\mu\mathrm{m}^2$. On a 5 mm × 5 mm substrate four such structures can be patterend. Fig. 1(b) shows a zoom-view of one small TMR-turret. The measurement current flows from the main bottom electrode path, up through the turret with the magnetic electrode layers and the tunnel barrier perpendicular to the sample surface, and then back through the upper narrow-waisted gold electrode.

EXPERIMENTAL RESULTS AND DISCUSSION

Magnetization

The magnetization as a function of temperature and applied magnetic field of the multilayer samples has been measured before any lithographic step i.e. the whole chip was measured. To investigate the influence of the lithographic patterning process, one sample has been patterned into a 3 mm × 3 mm square. The magnetization behavior of the sample before and after patterning was almost identical. This means that the magnetization data as measured for the whole chip is valid approximately also for the patterned TMR-contacts.

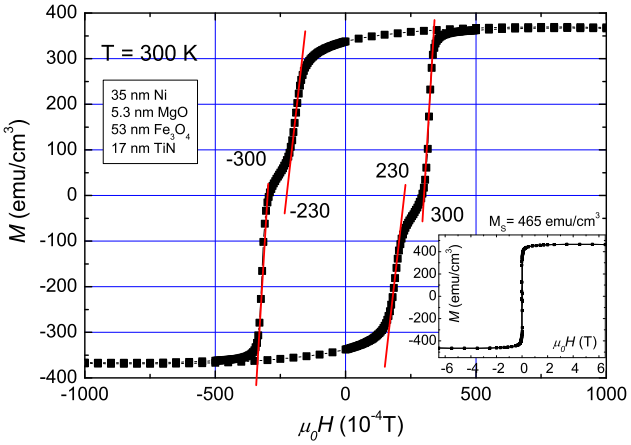

Figure 2: Magnetization behavior of a TiN/Fe_3O_4/MgO/Ni multilayer. Inset: Same measurement up to 6 T.

First, we consider the saturation magnetization M_S.

The inset of Fig. 2 shows a magnetization measurement of a TiN/Fe_3O_4/MgO/Ni multilayer up to above 6 T. For single reference layers of magnetite and Ni we have measured $M_S \approx 453\,\mathrm{emu/cm^3}$ resp. $M_S \approx 495\,\mathrm{emu/cm^3}$ at room temperature. Knowing the film thicknesses within the multilayer consisting of 53 nm magnetite, 5.3 nm MgO, and 35 nm Ni on top of a 17 nm TiN buffer layer, a saturation magnetization of $470\,\mathrm{emu/cm^3}$ is expected which is in excellent agreement with the measured value of $465\,\mathrm{emu/cm^3}$. Together with the clear step-like shape of the hysteretic $M(H)$-curve this is an indication of nearly ideal ferromagnetic order in the electrode layers of the multilayer structures. This is important with respect to the formation of magnetic domains or glass-like behavior which both is unfavorable for the device performance. Note, that M_S of the thin films is close to the values measured in bulk samples.

For an ideal switching behavior of a TMR-device it is important that both electrodes switch separately at different fields. Within this field range, a stable antiparallel configuration of the magnetization of the electrodes can be achieved. The difference in resistance of the stable states with perfect parallel and antiparallel order of the magnetization of the electrodes is a key precondition for high TMR-effects [15].

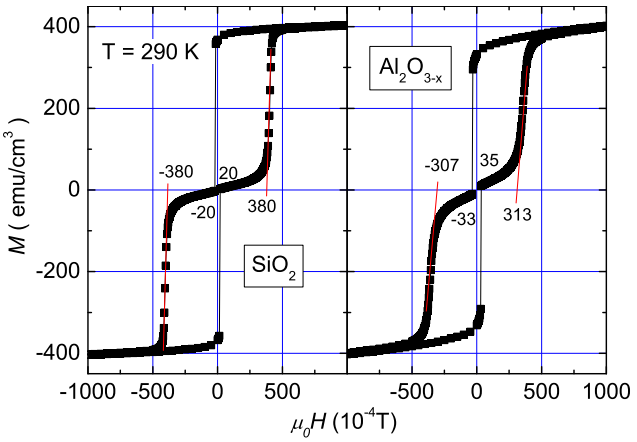

Figure 3: $M(H)$ at room temperature for two different barrier materials. Left panel: Fe_3O_4/SiO_2/Ni. Right panel: TiN/Fe_3O_4/Al_2O_{3-x}/Ni.

We first discuss the behavior of MgO barriers. As shown in Fig. 2, for a barrier of 5.3 nm MgO the difference of the switching fields of Fe_3O_4 and Ni is only about 7 mT at room temperature. At lower temperatures (210 K and 150 K) the electrodes switch together around applied fields of 30 mT. These switching fields are far away from the typical coercive fields for Ni thin films (≈ 7 mT at 5 K [$M_S(5\,\mathrm{K}, 7\,\mathrm{T}) \approx 560\,\mathrm{emu/cm^3}$] and ≈ 0.25 mT at room temperature [$M_S(290\,\mathrm{K}, 7\,\mathrm{T}) \approx 495\,\mathrm{emu/cm^3}$]) which are much smaller as observed in the multilayer structure. It is evident that the electrodes are strongly coupled through the MgO barrier layer, behaving like almost one ferromagnetic layer.

To investigate the magnetic coupling through the MgO tunnel barrier in more detail, the same measurements have been repeated with a thicker barrier layer (21 nm). From atomic force microscopy and x-ray reflectometry measurements indicating a surface roughness below one nm (root mean square), we exclude that short circuits exist through the barrier. Interesting enough, the same coupling phenomenon is observed again. At this moment, we can only speculate about the origin of this phenomenon. The first possibility is that Fe diffuses into the MgO barrier and vice versa leading to a diluted magnetic system $Mg_{1-x}Fe_xO$. While such interdiffusion has only been observed after annealing processes at much higher temperatures [16], here the PLD process with a cloud of ≈ 50 eV particles could drive interdiffusion between the two well lattice matched systems MgO and Fe_3O_4. In contrast, electron beam evaporation or plasma assisted molecular beam epitaxy [16] deals with almost thermalized atoms. Within this model, at increasing temperature the coupling is decreased due to the decreased order of the magnetic insulating layer. The second possible origin of the magnetic coupling through the MgO barrier, is related to recent ideas about new types of ferromagnets due to the presence of specific point defects in low concentration [17]. Point defects due to Mg vacancies within such models are responsible for ‚local' magnetic moments. Also, oxygen deficient systems might in a similar way lead to ferromagnetic behavior. However, for the purpose of TMR devices, non-magnetic insulating tunnel barriers are needed that decouple the electrodes effectively.

Fig. 3 shows magnetization measurements of two samples consisting of 47 nm Fe_3O_4 / 5 nm SiO_2 / 40 nm Ni resp. 14 nm TiN / 49 nm Fe_3O_4 / 2.5 nm Al_2O_{3-x} / 32 nm Ni. In contrast to the samples with MgO tunnel barrier layer, these samples show a clear separated magnetization switching of the electrodes at all temperatures. The coercive field of the Ni layer is slightly increased as compared to the values of the single thin reference nickel film. This effect is due to residual coupling through the thin insulating barrier. For the Al_2O_{3-x} barrier the switching steps are more rounded than for the case of SiO_2 indicating that magnetic domains do not switch simultaneously within the whole interface region. The difference between SiO_2 and Al_2O_{3-x} is that SiO_2 and Ni is evaporated directly on top of magnetite. In the case of Al_2O_{3-x}, first an Al layer is deposited which is then oxidized. It is this oxidation step that also can affect the magnetite top layer leading to the observed non-ideal switching behavior.

$R(T)$

A first crucial test for the reproducibility of the tunnel barrier is the investigation of the product of junction

area A	$2p$-resistance	$4p$-resistance	$R_{4p} \cdot A$
10μm x 10μm	172 Ω	66 Ω	$6.6{\cdot}10^{-9}$ Ωm^2
10μm x 20μm	292 Ω	36 Ω	$7.1{\cdot}10^{-9}$ Ωm^2
20μm x 20μm	407 Ω	23 Ω	$9.1{\cdot}10^{-9}$ Ωm^2
20μm x 40μm	539 Ω	5.0 Ω	$4.0{\cdot}10^{-9}$ Ωm^2

Table I: Resistance-times-area-product of a TMR-samples having a 2.5 nm Al_2O_{3-x} barrier at room temperature.

area A and junction resistance. We have listed in Table I the measured room temperature values for a sample consisting of four contacts with different size but with the same 2.5 nm Al_2O_{3-x} barrier. The four-point-resistance R_{4p} of the contacts scales inverse to their area, and the resistance-times-area-product $R_{4P} \cdot A$ of all contacts is in the same range of $10^{-9}\,\Omega\mathrm{m}^2$. This shows, that all contacts are approximately of the same quality, independent on their size. This implies that the insulating SiO_2 coating at the border of the TMR-turrets indeed suppresses leakage currents. The values obtained here for Al_2O_{3-x} barriers are comparable to the results of other groups. Chen *et al.* found 1-230$\cdot10^{-9}\,\Omega\mathrm{m}^2$ at room temperature for simple oxidized barriers and four times higher values with plasma oxidation [18]. The junctions with the higher resistance times area product also had a significantly higher TMR effect [18]. This shows that an optimization of the Al oxidation process is a crucial step in the fabrication of a TMR device.

Fig. 4 shows resistance versus temperature curves of TMR-contacts with different tunnel barriers and a magnetite reference film for comparison. All curves are normalized to their room temperature resistance. The absolute resistance values are in the range of 5 Ω - 10 kΩ at room temperature. Due to the Verwey transition the resistance of the magnetite layer increases several orders of magnitude at approximately $T_V \approx 120\,\mathrm{K}$ [19]. For

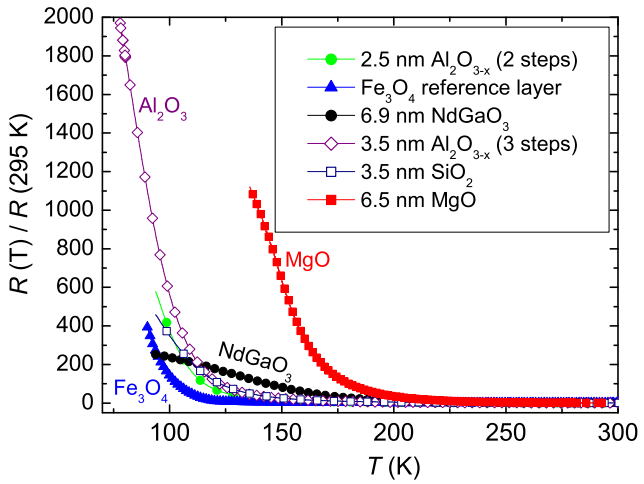

Figure 4: $R(T)$ of TMR-contacts with different tunnel barriers in comparison.

barrier	thickness d	fit value d	ϕ at 160 K	ϕ at 295 K
$NdGaO_3$	6.9 nm	0.9 nm	5 eV	2 eV
$SrTiO_3$	2.8 nm	1.4 nm	1.6 eV	1.5 eV
SiO_2	3.5 nm	1.4 nm	1.2 eV	0.9 eV
MgO	6.5 nm	2.3 nm	0.9 eV	0.7 eV
Al_2O_{3-x}	2.5 nm	1.6 nm	0.7 eV	0.6 eV

Table II: Effective barrier height ϕ and width d (at 160 K) of the tunnel barrier in samples with different barrier materials as derived using the Simmons model [20].

the multilayer systems the resistance increases already at temperatures above T_V. This effect is most pronounced for the MgO barrier layer where the resistance starts to increase strongly at around 175 K. As discussed above, it is likely that especially the MgO barrier has a high density of dislocation centers. Therefore, the increase of resistance is most likely due to the suppression of thermally activated hopping conduction through the insulating barrier.

Here, we briefly estimate the influence of the magnetite electrode on the resistance of the whole turret structure. Assuming homogeneous current feed into the turret due to the well conducting TiN buffer layer, and knowing the resistivity of magnetite, a resistance of $5.6{\cdot}10^{-3}\,\Omega$ at room temperature is expected for a 20 x 20 μm^2 turret. It is evident that the effect of Fe_3O_4 is negligible at least at temperatures not to close to the Verwey transition. In the case of inhomogeneous current feed, the influence of the magnetite electrode can no longer be neglected. It is therefore necessary for a precise determination of the barrier properties to have a low resistance buffer layer beneath the Fe_3O_4 electrode.

$U(I)$

To further investigate the tunnel barrier properties, $U(I)$-curves were measured and fitted to the Simmons model assuming a trapezoid barrier shape [20]. From this fit, the effective barrier height ϕ and barrier width d can be determined in the case $eV \ll \phi$. Due to the large barrier heights ϕ in the eV-range, the measurement current has to be chosen high enough in order to observe non-linearities. For samples with low resistance of only few Ω the application of large currents is of course not possible. The non-linearity in $U(I)$ is most pronounced at low temperatures ($\approx 160\,\mathrm{K}$), and is replaced by almost Ohmic behavior at room temperature due to increased thermally activated transport via defect states. Using the Simmons model the $U(I)$ curves could be fitted very satisfactory. The results for the effective barrier height ϕ and width d after the Simmons-model for the different tested barrier materials are listed in Table II. $NdGaO_3$ with 5 eV has the highest barrier, and Al_2O_{3-x}

with 0.7 eV the lowest barrier height at the Fermi level. These values are well comparable to the results of other groups, see for example $\phi = 0.9\,\mathrm{eV}$ for MgO [21]. The value for the effective barrier width as obtained from the Simmons fit is in most cases considerably smaller than the nominal barrier thickness. It becomes clear from Table II that for Al_2O_{3-x} barriers the fit parameter d is closest to the nominal barrier thickness indicating that Al_2O_{3-x} seems to be the best material for obtaining thin and at the same time well insulating barriers. For comparison, in order to achieve comparable barrier properties using MgO a several times thicker layer has to be used. It can be assumed that the increased barrier thickness leads to increased spin scattering reducing the TMR effect. This effect is indeed observed as shown below. The reason that Al_2O_{3-x} is the most favorable barrier is most likely due to the fact that during electron beam evaporation first an almost complete surface wetting is achieved with elementary Al.

TMR-effect

With $R(H)$-measurements in 4-point-technique the TMR-effect as defined in equation 1 was determined for the different barrier materials at different temperatures between 160 K and 300 K:

$$TMR = \frac{R_{ap} - R(H)}{R_p}. \qquad (1)$$

R_{ap} is the resistance in the anti-parallel magnetization configuration of the electrodes, which corresponds to the maximum resistance in figure 5. R_p is the resistance in the parallel magnetization configuration of the electrodes, which corresponds to the minimal resistance at 0.1 Tesla.

The samples with MgO and SiO_2 barrier exhibited only a small positive TMR-effect $< 0.5\%$ at low temperatures.

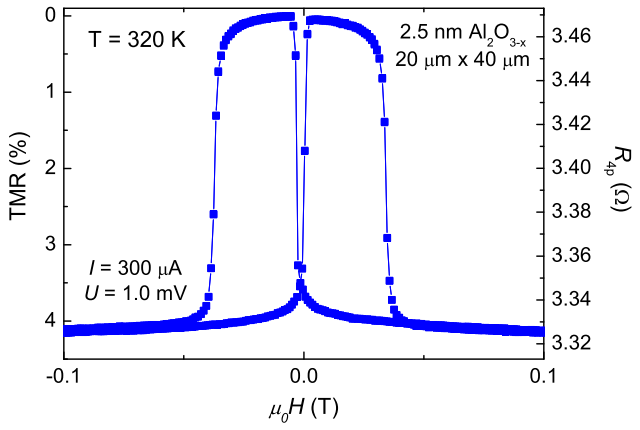

Figure 5: TMR-effect at room temperature of a sample with 2.5 nm Al_2O_{3-x} barrier. The barrier was oxidized in a 1-step process.

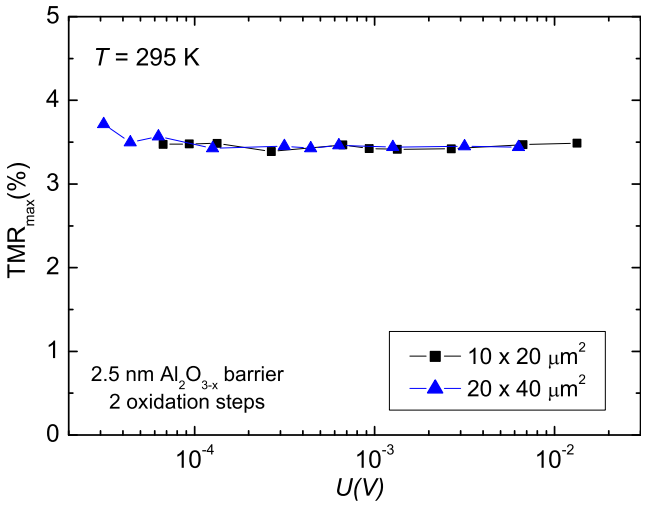

Figure 6: TMR-effect versus voltage for samples with 2.5 nm Al_2O_{3-x} barrier at room temperature.

Samples with $SrTiO_3$ and $NdGaO_3$ barrier showed nearly no TMR-effect at all. In these multilayers a small negative conventional magnetoresistance was observed as is the case for magnetite thin films. This indicates that the electrode properties dominate the measurements in these contacts. It has been shown by other groups [22, 23] that it is possible to obtain TMR-behavior using these barrier materials at low temperatures. But in the case of magnetite electrodes however, it is not easy to find good TMR-behavior below T_V due to the strong increase of resistance.

The samples with Al_2O_{3-x} barrier showed reproducibly a clear positive TMR-effect with almost ideal, symmetric switching behavior as shown in Fig. 5. The TMR effect is observable in the whole measured temperature range from 150 K to 350 K. At room temperature up to 5% resistance change was found. A second oxidation process in our case did not increase the TMR effect. The TMR-behavior is in agreement with the analysis of the junction properties. Al_2O_{3-x} provides a good insulator for the thinnest barriers with the lowest amount of defect states leading to magnetic decoupled electrodes and reduced spin scattering at the same time. Note that the increase of resistance for antiparallel electrode magnetization (positive TMR-effect) confirms the negative spin-polarisation of Fe_3O_4. Since Ni and Fe_3O_4 both have negative spin polarisation, the observed behavior is expected. For an electrode with positive spin polarisation as the double exchange material $La_{0.7}Sr_{0.3}MnO_3$, a negative TMR-effect is expected, and indeed observed [24, 25].

It is well known that for samples with a high density of defect states, at increased voltages the TMR effect decreases due to inelastic spin scattering transport processes in the barrier [26]. In Fig. 6 the maximal TMR-effect is plotted versus the applied tunnel voltage. The different measurement points were obtained for different

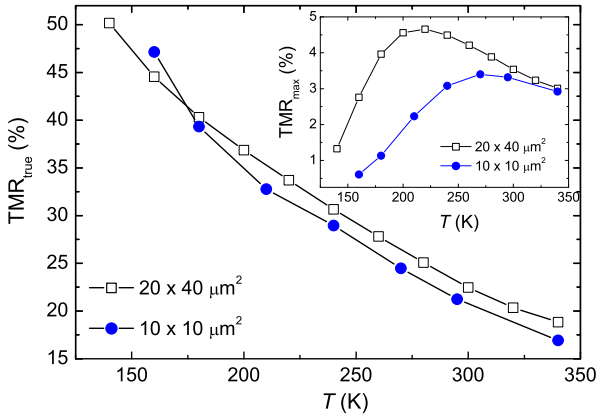

Figure 7: ‚True' TMR effect and maximal TMR effect versus temperature for samples with 2.5 nm Al_2O_{3-x} barrier.

applied currents. It is clear that over more than two orders of magnitude (in the range of 10^{-5} V to 10^{-2} V) no change of the TMR effect is observed. This result implies that in the observed voltage range no additional inelastic transport channels with spin scattering are opened. The Al_2O_{3-x} barrier acts as a good insulating barrier where the defect states do not dominate the transport behavior in the low-voltage regime.

The inset of Fig. 7 shows the temperature dependence of the maximal TMR-effect $TMR_{\max}$ of two samples with 2.5 nm Al_2O_{3-x} barrier. The junction size and the number of oxidation steps varies for both junction. The larger junction ($20 \times 40\,\mu m^2$) has a two-step oxidized barrier [27], while the smaller junction ($10 \times 10\,\mu m^2$) has a one-step oxidized barrier. $TMR_{\max}(T)$ has a non-linear behavior with a maximum the position of which depends on deposition details. For higher temperatures above approximately 280 K all curves converge. It is obvious that only a decrease of magnetization/spin polarisation in the tunneling electrodes and thermally assisted inelastic spin scattering processes lead to a decreased TMR effect. $TMR_{\max}(T)$ is expected to be a continously decreasing function with increasing temperature. The reason that experimentally a maximum is observed in $TMR_{\rm meas}(T)$ can be explained within a simple model assuming a constant series resistance R_S in the TMR-turret in addition to the barrier resistance R_B . The series resistance is not affected by the change of spin polarisation of the electrodes producing the ‚real' TMR-effect by switching R_B. For the measured TMR effect $TMR_{\rm meas}$ one obtains:

$$TMR_{\rm meas} = \frac{\Delta R}{R_B + R_S} \qquad (2)$$

This value can easily be related to the ‚true' TMR effect $TMR_{\rm true}$:

$$TMR_{\rm true} = \frac{\Delta R}{R_B} = TMR_{\rm meas}\left(1 + \frac{R_S}{R_B}\right) \qquad (3)$$

Because the measured 4-point-resistance $R_{4\rm p}$ of the TMR-structure is the sum of the barrier resistance R_B and the series-resistance R_S, eq. 3 can be rewritten as

$$TMR_{\rm true} = \frac{\Delta R}{R_B} = TMR_{\rm meas}\left(1 + \frac{R_{4\rm p} - R_B}{R_B}\right). \qquad (4)$$

While $R_{4\rm p}$ is a measured quantity, the value of R_B has to be estimated. By assuming a realistic resistance times area product of approximately $10^{-9}\,\Omega m^2$, for R_B one obtains roughly $10\,\Omega$. The resulting $TMR_{\rm true}(T)$ is shown in Fig. 7, and has the expected continuously (almost linearly) decreasing behavior. Between 150 K and 300 K $TMR_{\rm true}$ decreases by more than 50% while the corresponding decrease in magnetization is only about 10% for Fe_3O_4 and 11.6% for Ni. According to the Jullière model [15], this accounts for a decrease in $TMR_{\rm true}$ of 28% assuming that magnetization translates directly into spin polarisation. Having in mind the results of $U(I)$ at different temperatures and also the reduced magnetic coupling, the difference to the estimated value of $TMR_{\rm true}$ can be understood due to the increase in spin-scattering at defect states in the tunnel-barrier.

SUMMARY

We have successfully prepared magnetic tunnel junctions with sizes of $10 \times 10\,\mu m^2$ to $20 \times 40\,\mu m^2$ with optical lithography and ion beam etching. The bottom electrodes consist of epitaxial magnetite thin films on MgO substrates using a TiN buffer-layer. As tunnel barrier five different materials have been investigated. Thin nickel films have been used for the top electrode.

The analysis of $M(H)$ curves showed that for MgO barriers the electrodes couple magnetically even for high barrier thicknesses (up to 21 nm). Al_2O_{3-x} as barrier leads to a clearly separated magnetization switching of the electrodes with more rounded steps than in the case of SiO_2.

$R(T)$- and $U(I)$-measurements of the tunnel-contacts showed a strong decrease of the insulating behavior of the barriers with increasing temperature. This may be due to tunneling via thermal activated defect states in the barrier layer.

The TMR-contacts with MgO and SiO_2 barrier exhibited only a small effect $< 0.5\%$ at low temperatures < 200 K. Samples with $SrTiO_3$ and $NdGaO_3$ barrier showed nearly no TMR-effect at all. The tunnel-contacts with Al_2O_{3-x} barrier showed reproducibly a clear TMR-effect with ideal, symmetric switching behavior. The effect was visible in the whole investigated temperature range from 150 K to 350 K. At room temperature up to 5% resistance change was found. Almost no influence of the applied voltage on the size of the TMR-effect in the studied voltage range from 10^{-5} V to 10^{-2} V is observed. The temperature dependence of the as measured TMR-effect shows a pronounced maximum. This can be ex-

plained by an additional series-resistor in the TMR-turret combined with the decrease of the spin-polarization of the electrodes at increasing temperature, and by increased spin-flip-scattering at higher temperatures. Further experiments are needed to specify the exact value of the spin-polarization of the magnetite electrode at room temperature. But it is obvious from the presented data, that magnetite has high spin-polarization and certainly is an interesting candidate as a material for further spinelectronic devices at room temperature.

We would like to thank J. Schuler for help with the electron beam evaporation and the lithography. This work was supported in part by the Deutsche Forschungsgemeinschaft (project No.: Al/560) and the BMBF (project No.: 13N8279).

* Electronic address: Daniel.Reisinger@wmi.badw.de
† Electronic address: Lambert.Alff@wmi.badw.de

[1] A. Ney, C. Pampuch, R. Koch, and K. H. Ploog, Nature **425**, 485 (2003).
[2] Z. Zhang and S. Satpathy, Phys. Rev. B, **44**, 13319 (1991).
[3] H. T. Jeng and G. Y. Guo, Phys. Rev. B, **65**, 094429 (2002).
[4] Yu. S. Dedkov, U. Rüdiger, and G. Güntherodt, Phys. Rev. B **65**, 064417 (2002).
[5] X. W. Li, A. Gupta, Gang Xiao, W. Qian, and V. P. Dravid, Appl. Phys. Lett. **73**, 3282 (1998).
[6] K. Ghosh, S. B. Ogale, S. P. Pai, M. Robson, E. Li, I. Jin, Z. Dong, R. L. Greene, R. Ramesh, and T. Venkatesan, Appl. Phys. Lett. **73**, 689 (1998).
[7] P. Seneor, A. Fert, J.-L. Maurice, F. Montaigne, F. Petroff, and A. Vaurès, Appl. Phys. Lett. **74**, 4017 (1999).
[8] P. J. van der Zaag, P. J. H. Bloemen, J. M. Gaines, R. M. Wolf, P. A. A. van der Eijden, R. J. M. van de Veerdonk, and W. J. M. de Jonge, J. Magn. Magn. Mater. **211**, 301 (2000).
[9] H. Matsuda, M. Takeuchi, H. Adachi, M. Hiramoto, N. Matsukawa, A. Odagawa, K. Setsune, and H. Sakakima, Jpn. J. Appl. Phys. **41**, L387 (2002).
[10] J. S. Moodera, and G. Mathon, J. Magn. Magn. Mater. **200**, 248 (1999).
[11] J. Klein, C. Höfener, L. Alff, and R. Gross, Supercond. Sci. Technol. **12**, 1023 (1999); see also J. Magn. Magn. Mater. **211**, 9 (2000).
[12] D. Reisinger, B. Blass, J. Klein, J. B. Philipp, M. Schonecke, A. Erb, L. Alff, and R. Gross, Appl. Phys. A **77**, 619 (2003).
[13] D. Reisinger, M. Schonecke, T. Brenninger, M. Opel, A. Erb, L. Alff, and R. Gross, J. Appl. Phys. **94**, 1857 (2003).
[14] D. Reisinger, P. Majewski, M. Opel, L. Alff, and R. Gross, preprint (2004).
[15] M. Jullière, Phys. Lett. A **54**, 225 (1975).
[16] K. A. Shaw, E. Lochner, and D. M. Lind, J. Appl. Phys. **87**, 1727 (2000).
[17] I. S. Elfimov, S. Yunoki, and G. A. Sawatzky, Phys. Rev. Lett. **89**, 216403 (2002).
[18] E. Y. Chen, R. Whig, J. M. Slaughter, D. Cronk, J. Goggin, G. Steiner, and S. Tehrani, J. Appl. Phys. **87**, 6061 (2000).
[19] E. J. W. Verwey, Nature **144**, 327 (1939).
[20] J. G. Simmons, J. Appl. Phys. **34**, 1793 (1963).
[21] T. Kiyomura, Y. Maruo, and M. Gomia, J. Appl. Phys. **88**, 4768 (2000).
[22] J. M. De Teresa, A. Barthélémy, A. Fert, J. P. Contour, F. Montaigne, and P. Seneor, Science **286**, 507 (1999).
[23] M. Bowen, M. Bibes, A. Barthélémy, J.-P. Contour, A. Anane, Y. Lemaitre, and A. Fert, Appl. Phys. Lett. **82**, 233 (2003).
[24] J. M. De Teresa, A. Barthélémy, A. Fert, J. P. Contour, R. Lyonnet, F. Montaigne, P. Seneor, and A. Vaurès, Phys. Rev. Lett. **82**, 4288 (1999).
[25] G. Hu and Y. Suzuki, Phys. Rev. Lett. **89**, 276601 (2002); G. Hu, R. Chopdekar, and Y. Suzuki, J. Appl. Phys. **93**, 7516 (2003).
[26] C. Höfener, J.B. Philipp, B. Wiedenhorst, J. Klein, L. Alff, A. Marx, B. Büchner, and R. Gross, Europhys. Lett. **50**, 681 (2000).
[27] The barrier is deposited in two steps, and after each deposition step oxidation is performed.